Electrical Power and Energy Systems 164 (2025) 110430

Contents lists available at ScienceDirect

International Journal of Electrical Power and Energy Systems

journal homepage: www.elsevier.com/locate/ijepes

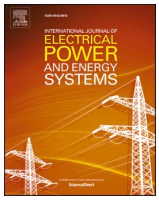

Enlarged operational area of an Interline DC power Flow controller via adaptive droop control for Multi-Terminal HVDC systems

Mirhamed Pourmirasghariyan [a,*], G.B Gharehpetian [b], Oriol Gomis-Bellmunt [c], David Campos-Gaona [a], Panagiotis N. Papadopoulos [d]

[a] Department of Electronic and Electrical Engineering (EEE), University of Strathclyde, Glasgow, G1 1XQ, UK
[b] Department of Electrical Engineering, Amirkabir University of Technology, Tehran 15875-4413, Iran
[c] CITCEA-UPC, Universitat Politècnica de Catalunya, Barcelona 08028, Spain
[d] School of Electrical and Electronic Engineering, The University of Manchester, Manchester, M60 1QD, UK

ARTICLE INFO

Keywords:
Adaptive Droop Control
HVDC
IDC-PFCs
MMCs
Optimal Power Flow

ABSTRACT

The effective performance of Interline DC Power Flow Controllers (IDC-PFCs) in Modular Multilevel Converters (MMC)-based High Voltage Direct Current (HVDC) grids is restricted by 1) the current limitation of the HVDC cables/lines, 2) the HVDC buses' DC voltages and 3) the IDC-PFC capacitor's DC voltage limit. The pivotal remedy for this issue is to utilize an adaptive droop control for the MMCs that varies its droop gain to maximize the IDC-PFC operation range. In this paper, 3D curves of the IDC-PFC's important characteristics are used to assess the flexibility of the IDC-PFC control. By using this approach, a new degree of freedom for IDC-PFC controllability is achieved. The performance of the optimal-adaptive-droop-controlled strategy presented in this paper is validated using power flow studies. The results demonstrate that a wider operational area is conceivable for the IDC-PFC when this technique is applied as a combination of MMC converters' droop control and IDC-PFC duty cycle.

1. Introduction

1.1. Motivations

Future meshed Modular Multilevel Converter (MMC)-based High Voltage Direct Current (HVDC) grids, targeting the integration of Renewable Energy Sources (RESs) into main power systems promise enhanced integration stability, without concerns regarding reactive power requirements [1–3]. Moreover, to enhance the flexibility of the Power Flow (PF) of the MMC-based HVDC grids, the Interline DC Power Flow Controllers (IDC-PFCs) have been proposed in the research literature [4–6]. Although IDC-PFCs are a promising technology, the region of the IDC-PFC's operation is somehow limited. In fact, the operation of IDC-PFCs is highly dependent on the current limitation of HVDC cables/lines, the DC voltage limitations of interconnected buses, and the IDC-PFC capacitor's DC voltage boundaries [5].

Therefore, the main goal of the present paper focuses on introducing a new degree of freedom to overcome the mentioned issues of the IDC-PFCs' operation in MMC-based HVDC grids and enhancing IDC-PFC's contribution to DC-PF.

1.2. Literature Review

There is a growing interest in interconnecting Voltage Source Converters (VSCs) or MMCs for the purpose of achieving Multi-Terminal HVDC structure (MT-HVDC) grids, or meshed HVDC grids. The meshed HVDC grids have many HVDC cables/lines with complex control systems and operation modes [7] and [8]. One major concern of the MT-HVDC grids is Power Flow studies. In case of poor control, congestion, and bottlenecks overloading would occur in HVDC cables/lines. Accordingly, DC-PFCs, which are equivalent to the Flexible AC Transmission System (FACTS) devices and have the same tasks, are introduced. DC-PFCs can manipulate the DC Power Flow (DC-PF) equations and bring about flexibility and controllability in power/current flow. Generally, DC-PFCs are known in three categories series, cascaded, and interline. Among these three categories, since the IDC-PFCs have a simple control system, structure, and economic advantages, they are under heavy attention [8]. The IDC-PFCs inject DC voltage in series into

* Corresponding author.
E-mail address: mirhamed.pourmirasghariyan@strath.ac.uk (M. Pourmirasghariyan).

https://doi.org/10.1016/j.ijepes.2024.110430
Received 7 September 2024; Received in revised form 10 November 2024; Accepted 15 December 2024
Available online 20 December 2024

their interconnected HVDC cables/lines by setting appropriate control variables (duty cycle) and consequently vary the current/power of their interconnected HVDC cables/lines.

There are several methods for power sharing and current control in MT-HVDC grids apart from the presence of DC-PFCs. One effective way that enables the operators to appropriately utilize the capacity of converters, is adaptive droop control. In [9], a generalized droop-control strategy has been proposed that has the ability to operate under three possible modes (constant power, constant voltage, and droop-controlled voltage-power) according to the demand of operators with rational power sharing. The generic method of [9] paves the way for easy maneuverability over three different operation modes. The authors of [10], have proposed a scheme for the droop control of VSCs that not only acts to reach a reasonable power-sharing but also avoids converters' power and DC voltage limit violations. The studied method of [10] is adaptive in which droop values of the converters are set automatically to reach a stable and safe operation for the system. Moreover, in [11], a droop control strategy has been introduced that considers frequency deviation and power sharing according to the characteristics of the voltage-current-frequency relationship. Also, in [12], the authors have developed a new coordinated-predictive droop control that avoids High Voltage Ride-Through (HVRT) by following an optimal droop coefficient. Further, the performance of droop techniques in terms of power sharing and transient stability, have been evaluated in [13].

The combination of droop control of MMCs/VSCs with the IDC-PFCs has some important advantages, which have never been studied in the previous droop-controlled strategies. Manipulating droop values of those converters in which an IDC-PFC is connected, can remove or at least mitigate the limitations of the IDC-PFC. More importantly, removing these limitations would pave the way to reach a more flexible, widened, and controllable operation of the IDC-PFCs and the grid as well. The aforementioned restrictions are dealt with partially in [5] by using only one degree of freedom (the duty cycle), however, a complete method for overcoming IDC-PFC limitations has not yet been proposed in the open literature. Therefore, this paper aims to overcome those restrictions with the help of adaptive droop control of IDC-PFC's interconnected converters. Consequently, an adaptive-optimal droop control strategy is introduced, which considers the mentioned limitations and adapts the converters' droop gains accordingly to widen the IDC-PFCs' operation capabilities.

1.3. Research Objectives and contributions

The contributions of this paper are as follows:

- In section II, an adaptive-droop-controlled strategy is proposed in which not only the DC voltage and power limits of the MMCs/VSCs are considered but also takes the limitations of the IDC-PFC into account. Hence, the droop gains of the MMCs/VSCs are set in the presence of IDC-PFCs within the DC network. By addressing these limitations, the duty cycle of the IDC-PFC can be swung extensively leading to a flexible operation.
- In section III, the influence of variable droop control on the behavior of an IDC-PFC in a three-terminal CIGRE HVDC test grid is evaluated. Here, the 3D characteristics of the IDC-PFC with two autonomous degrees of freedom (duty cycle of the IDC-PFC and the variable droop) are analyzed. Afterwards, the results are compared to those of the [5], and the benefits of the proposed strategy are discussed.
- In section V, an Optimal-Adaptive-Droop-Controlled Power Flow (OADC-PF) study is conducted in a steady-state situation. Optimal results for determining adaptive droop values mean the MMCs/VSCs are used to attain a successful IDC-PFC limitation removal.
- Finally, in section VI, dynamic and OADC-PF case studies are provided.

2. The IDC-PFC under adaptive droop control

2.1. Operation Principles of IDC-PFC

There are several recent publications regarding new topologies for IDC-PFC. However, in this paper, the basic topology presented in [14], is chosen to focus fundamentally on the effect that the variable droop gain has on the behavior of the IDC-PFC, as well as obtaining its 3D characteristics in the presence of duty cycle (D) and the new degree of freedom (K_{Droop}) which provides an adaptable gain for the droop controller.

Fig. 1 (a) illustrates the topology of the IDC-PFC, which is built up of a reduced dual H-bridge and a DC capacitor. The DC capacitor of the IDC-PFC can operate under positive or negative DC voltage, and its value ($\overline{E}_C$) is dependent on the voltages of its interconnected buses and the control variable setting D. The IDC-PFC is located through HVDC cable t (master cable) and HVDC cable u (slave cable) that injects predetermined-compensating voltages $U_{s,t} = (1-D)\overline{E}_C$ and $U_{s,u} = -D\overline{E}_C$ in series with the interconnected HVDC cables t and u, respectively, as shown in Fig. 1 (b). The performance of the IDC-PFC involves exchanging power between the two (master and slave) HVDC cables. Thus, the more compensating voltage injection increases through the main HVDC cable t, the more power/current flowing through the main HVDC cable t increases, and vice versa.

The IDC-PFCs are considered minor-sized converters in comparison with VSCs or MMCs. Therefore, the losses of the IDC-PFCs are slight (0.002 % losses of the MMCs') [15]. Hence, in this research, the IDC-PFCs are regarded to be lossless.

The HVDC cables are modeled as π−Lump model, and the parameters Z_t, Z_u, Y_t, and Y_u are the series impedance of HVDC cable t, series impedance of HVDC cable u, shunt admittance of HVDC cable t, and shunt admittance of HVDC cable u, respectively. Moreover, for the steady-state analysis of the grid, the cable parameters are R_t, G_t, R_u, and G_u which represent the HVDC cables t's and u's resistance and shunt conductance, respectively. Nevertheless, because the existence of the shunt admittance does not participate in PF results significantly, thus, they are crowded out of the formulations (hereafter) [16].

Based on Fig. 1 (a), considering that the IDC-PFC is placed between buses i, j, and k, the current flowing from bus-i (I_i) has two possible paths to flow between the HVDC cable t and HVDC cable u. There are two switching combinations, one for a positive current passage pair and the other one for a negative current passage pair. The switching combinations represented in Fig. 1 (a) are called positive current pairs in which the switches ($\{S_2, S_4, S_6\}$) and the diodes ($\{D_1, D_3, D_5\}$) are utilized. For the negative current directions, the switches ($\{S_1, S_3, S_5\}$) and the diodes ($\{D_2, D_4, D_6\}$) are used, for further information refer to [5]. For the current directions shown in Fig. 1 (a), the current of HVDC cable t (I_{ij}) passes through the switches ($\{D_1, \overline{E}_C, S_4\}$ and $\{S_2, \overline{E}_C, D_3\}$), while for the current of HVDC cable u (I_{ik}) the switches ($\{S_2, \overline{E}_C, D_5\}$ and $\{D_1, \overline{E}_C, S_6\}$) are involved. Considering, the duty cycle (D) for the closed state of the switches ($\{S_2, S_4\}$) for the current (I_{ij}) passage, and the closed state of the switches ($\{S_2, S_6\}$) with the complementary duty cycle ($1-D$) for the current (I_{ik}) passage, the average current passing through the IDC-PFC's capacitor ($\overline{I}_C$) must be zero. Under the given circumstances, the average current of the capacitor can be obtained as:

$$\overline{I}_C = \frac{1}{T}\int_0^T I_C dt = \frac{1}{T}(-DI_{ij} + (1-D)I_{ik}) \tag{1}$$

The parameter T and $\overline{I}_C$ are the operation cycle of the IDC-PFC and average IDC-PFC capacitor's current, respectively. The average current needs to be zero ($\overline{I}_C = 0$) for the stable operation of the IDC-PFC. Then, one can achieve:

$$\overline{I}_C = 0 \rightarrow D = \frac{I_{ij}}{I_{ij} + I_{ik}} \tag{2}$$

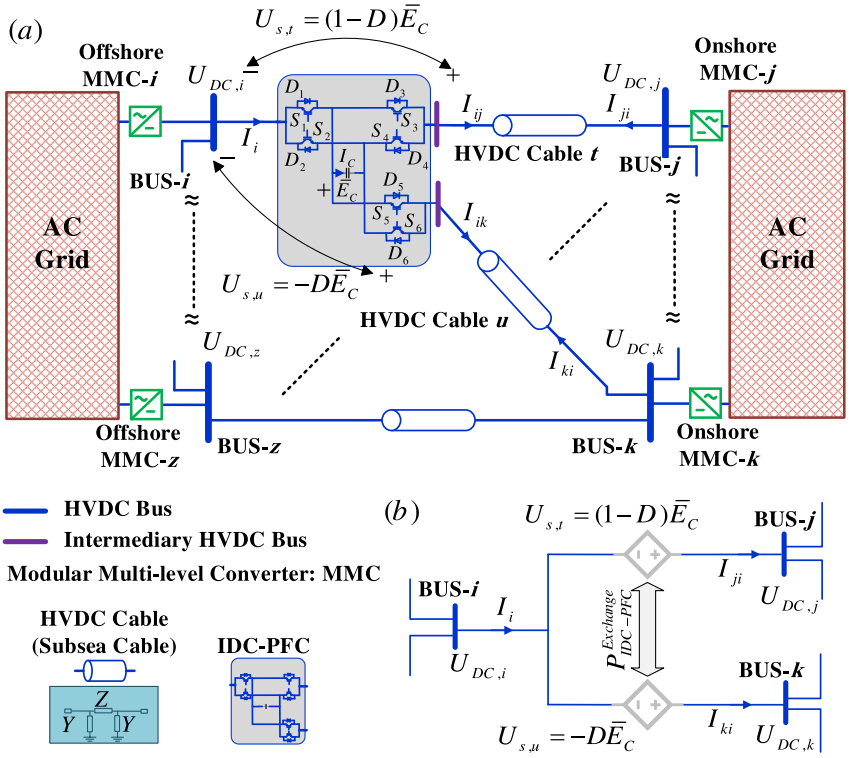

Fig. 1. (a) IDC-PFC installed between HVDC cables *t* and *u* in a meshed HVDC grid, and (b) IDC-PFC modeled by dependent voltage sources through its interconnected HVDC cables *t* and *u*.

With simple KVL/KCL law and neglecting the shunt admittance (Y), the currents of HVDC cable t (I_{ij}) and HVDC cable u (I_{ik}) can be achieved as follows:

$$I_t = I_{ij} = -I_{ji} = \frac{1}{Z_t}((U_{DC,i} - U_{DC,j}) + (1-D)\bar{E}_C) \tag{3}$$

$$I_u = I_{ik} = -I_{ki} = \frac{1}{Z_u}((U_{DC,i} - U_{DC,k}) - D\bar{E}_C) \tag{4}$$

The parameters $U_{DC,i}$, $U_{DC,j}$, $U_{DC,k}$, $\bar{E}_C$, I_t, and I_u are the voltage of bus-*i*, voltage of bus-*j*, voltage of bus-*k*, IDC-PFC's capacitor's DC voltage, current of HVDC cable *t*, and current of the HVDC cable *u*, respectively. Now, by substituting equations (3) and equation (4) into equation (2) and further manipulation, the IDC-PFC's capacitor's DC voltage can be obtained:

$$\bar{E}_C = T_i U_{DC,i} + T_j U_{DC,j} + T_k U_{DC,k} \tag{5}$$

$$T_i = \frac{DZ_t - (1-D)Z_u}{Z_t D^2 + Z_u(1-D)^2} \tag{6}$$

$$T_j = \frac{(1-D)Z_u}{Z_t D^2 + Z_u(1-D)^2}, T_k = \frac{-DZ_t}{Z_t D^2 + Z_u(1-D)^2}$$

The terms T_i, T_j, and T_k are the coefficients that relate the dependency of the IDC-PFC's capacitor on the duty cycle (D) and its interconnected bus voltages ($U_{DC,i}$, $U_{DC,j}$, and $U_{DC,k}$).

Moreover, the powers of the IDC-PFC interconnected HVDC cables/lines (t and u) are expressed, as follows:

$$P_{s,t} = U_{s,t}I_t, P_{s,u} = U_{s,u}I_u; U_{s,t} = (1-D)\bar{E}_C, U_{s,u} = -D\bar{E}_C \tag{8}$$

$$P_{IDC-PFC}^{Exchange} = P_{s,t} + P_{s,u} \tag{9}$$

The symbols $P_{s,t}$ and $P_{s,u}$ are the manipulated power of the HVDC cable *t*, and the manipulated power of the HVDC cable *u*, respectively. Additionally, the parameter $P_{IDC-PFC}^{Exchange}$ presents the exchanged power between the HVDC cables *t* and *u*.

According to the equation (3) and Fig. 1 (b), increasing voltage injection into HVDC cable t ($U_{s,t} = (1-D)\bar{E}_C$)), will increase the current flowing through the cable. Moreover, based on the active power balance condition, any increment in HVDC cable *t* current will reduce the current of HVDC cable *u*, and vice versa. With the given description and based on equation (9), a positive value for $P_{IDC-PFC}^{Exchange}$ means the power is exchanged from the HVDC cable *u* to the HVDC cable *t*, and vice versa.

2.2. Necessity of Integrating IDC-PFC characteristics into the adaptive droop gains of the MMCs/VSCs

The IDC-PFC operation has some restrictions. Regarding the fact that the IDC-PFC only operates by one degree of freedom (duty cycle), it might face some limitations including interconnected DC voltages of its interconnected buses, IDC-PFC capacitor's DC voltage violation, and current limitations. Hence, the duty cycle of the IDC-PFC would not be allowed to swing thoroughly from 0 to 1 or at least more extensively. Therefore, to avoid and escape these restrictions as much as possible, adaptive droop control of the IDC-PFC's interconnected converters could be a proper solution. The adaptive droop could mitigate this issue at some level. Therefore, in the present paper, a new strategy of adaptive droop control with the consideration of the IDC-PFCs is proposed and the important characteristics of the IDC-PFC with variable droop are analyzed.

2.3. Droop Concept

Considering the imbalance of the inflow power and outflow power, the generalized droop control equation of the converter with the droop (K_{Droop}) is presented below:

$$(P^* - P) + K_{Droop}(U_{DC}^* - U_{DC}) = 0 \tag{10}$$

In (10), the parameters U_{DC}, U_{DC}^*, P and P^* are the DC voltage, DC voltage reference, power, and power reference, respectively. Moreover, the symbol K_{Droop} represents the droop gain of an MMC. According to (10), an MMC-HVDC terminal might operate under one of the three modes: constant power, constant voltage, and voltage-power droop-controlled as shown in Fig. 2. The constant power mode maintains the power of the converter at a constant reference ($K_{Droop} = 0$) regardless of the DC voltage swing. For the constant DC voltage mode, the converter keeps the voltage at a fixed amount ($K_{Droop} = \infty$) regardless of power change. Finally, the droop-controlled mode is a combination of the two previous control modes in which the DC voltage of the converter changes according to a droop value (slope, m) for changing a specific power of the converter [11].

2.4. Integrating IDC-PFC into the formulations of adaptive droop of the MMCs/VSCs

Generally, there are some considerations for adaptive droop control of MMCs/VSCs. For example, even though the fixed droop gains of the converters are chosen in accordance with their ratings, this does not imply that they are operating at their full capacity. In other words, usually, there would be some available headroom for sharing the additional power imbalance. As such, one application of adaptive droop control is related to achieving reasonable power sharing among converters preventing converters' power limit violations. Moving forward, the second application is the voltage deviation of converters which is attained by proper droop swinging, which won't let the voltage violation happen. Hence, based on the given concepts, the below coefficients are considered for MMC's/VSC's droop gain that is not in connection with any IDC-PFC:

$$K_{Droop,i}^{Adaptive} = \lambda K_{Droop} \frac{\overbrace{P_{\max} - |P_i|}^{A}}{\underbrace{\sigma - |\Delta U_{DC,i}|}_{B}}; \Delta U_{DC,i} = 1 - |U_{DC,i}| \tag{11}$$

The term A indicates the available headroom of the i-th converter, while the term B denotes the DC voltage deviation of the i-th converter from its reference value and it is only considered to have a$\sigma = 5$ % deviation. The symbol λ is a user-defined factor to have further control over the droop value. In this equation, when the converter operates near its full capacity, the amount of A goes to zero and causes the converter to operate at constant power mode ($K_{Droop}^{Adaptive} = 0$). Furthermore, when the converter operates close to its DC voltage limit, the term B decreases and this causes the converter to operate at constant voltage mode ($K_{Droop}^{Adaptive} = \infty$).

On the other hand, whenever the IDC-PFC is connected to a droop-controlled converter, the problem of limitations of the IDC-PFC's operation could be avoided by assigning optimum adaptive droop control. Therefore, the following terms are also defined to bring the limitations of the IDC-PFC into the adaptive droop gain formulations where the IDC-PFC is installed:

$$K_{Droop,i}^{Adaptive} = \lambda_i K_{Droop,i} \times \frac{\overbrace{(P_{\max} - |P_i|)}^{A_i} \times \overbrace{((I_{\max,t} - |I_t|) + (I_{\max,u} - |I_u|))}^{C_i}}{\underbrace{(\sigma - |\Delta U_{DC,i}|)}_{B_i} \times \underbrace{(\overline{E}_{C,n} - |\overline{E}_C|)}_{d}} \tag{12}$$

$$K_{Droop,j}^{Adaptive} = \lambda_j K_{Droop,j} \times \frac{\overbrace{(P_{\max} - |P_j|)}^{A_j} \times \overbrace{(I_{\max,t} - |I_t|)}^{C_j}}{\underbrace{(\sigma - |\Delta U_{DC,j}|)}_{B_j} \times \underbrace{(\overline{E}_{C,n} - |\overline{E}_C|)}_{d}} \tag{13}$$

$$K_{Droop,k}^{Adaptive} = \lambda_k K_{Droop,k} \times \frac{\overbrace{(P_{\max} - |P_k|)}^{A_k} \times \overbrace{(I_{\max,u} - |I_u|)}^{C_k}}{\underbrace{(\sigma - |\Delta U_{DC,k}|)}_{B_k} \times \underbrace{(\overline{E}_{C,n} - |\overline{E}_C|)}_{d}} \tag{14}$$

The parameters $\overline{E}_{C,n}$, $I_{t,\max}$, and $I_{u,\max}$ are the nominal value of the IDC-PFC capacitor's DC voltage, the maximum current of HVDC cable t, and the maximum current of HVDC cable u, respectively. The above equations (12–14) represent the adaptive droop gains of the buses (i-th, j-th, and k-th) which are in connection with an IDC-PFC. The terms A_i, A_j, and A_k are responsible for reasonable power-sharing of the converters i-th, j-th, and k-th, respectively. Moreover, the terms B_i, B_j, and B_k for the converters i-th, j-th, and k-th, orderly, are considered for preventing DC voltage violations. Also, the symbols λ_i, λ_j, and λ_k are user-defined factors.

While the terms A_i, A_j, and A_k are associated with the powers of converters, the terms C_i, C_j, and C_k are defined to relate the droop gains of the converters to the currents of the IDC-PFC's interconnected cables. For the adaptive droop gain of i-th converter ($K_{Droop,i}^{Adaptive}$), the term C_i embeds the current limitations of the HVDC cables t and u ($I_{t,\max}$ and $I_{u,\max}$) into the adaptive droop gain of i-th converter which is in connection with HVDC cables t and u. The term C_i reduces the droop gain ($K_{Droop,i}^{Adaptive}$ (to prevent the i-th converter from having a major contribution to power-sharing when the currents of the IDC-PFC's interconnected HVDC cables are bottlenecked. In other words, when the HVDC cables t and u are overloaded, the term C_i tends to fall forcing the i-th converter to operate as a constant power bus ($K_{Droop,i}^{Adaptive} = 0$) not to absorb/inject power/current anymore. This procedure also happens for the adaptive droop gains ($K_{Droop,j}^{Adaptive}$ and $K_{Droop,k}^{Adaptive}$) by the terms C_j and C_k for the j-th, and k-th converters, respectively.

In addition, since the IDC-PFC capacitor's DC voltage (5) is dependent on the DC voltage of the buses i-th, j-th, and k-th, the term d is the same for the adaptive droop gains of all IDC-PFC's interconnected converters. If the value of $\overline{E}_C$ is close to its limit ($\overline{E}_{C,n}$), the droop gains rise ($K_{Droop,i}^{Adaptive} = K_{Droop,j}^{Adaptive} = K_{Droop,k}^{Adaptive} = \infty$) refusing the DC voltage limit of IDC-PFC's capacitor ($\overline{E}_C$) to be violated.

At this time, considering the droop value of bus-i in (12), the effect of the proposed nominator ($A_i \times C_i$) and the denominator ($B_i \times d$) on the

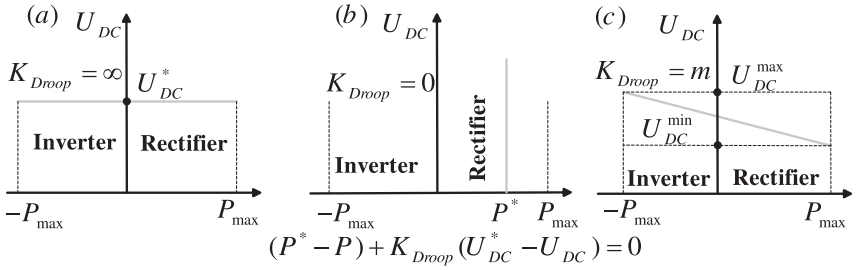

Fig. 2. Three possible operation modes of MMCs: (a) Constant voltage mode, (b) Constant power mode, and (c) Droop-controlled mode.

overall droop value can be investigated. Fig. 3 shows that when the nominator ($A_i \times C_i$) is low (close to zero), the converter is working close to its nominal power rating (therefore droop is low) and should not receive/inject more power, no matter what the denominator is. Based on Fig. 3, the less the term ($A_i \times C_i$) is, the less the droop gain will be, which means the loading of the bus-*i* and its interconnected cables/lines will be less. This will help the IDC-PFC not to be trapped in HVDC lines/cables and converter limits. On the other hand, when the denominator ($B_i \times d$) is low (close to zero), the droop value tends to rise rapidly to avoid voltage deviation of more than the specified amount, as seen in Fig. 3. This will prevent the IDC-PFC's capacitor's voltage from violating its limit which eventually will lead to further operational area for the IDC-PFC. At last, these advantages will enlarge the operational area of the IDC-PFC. The rest of the droop values of IDC-PFC's interconnected buses ($K^{Adaptive}_{Droop,j}$ and $K^{Adaptive}_{Droop,k}$) expose the same behavior.

Moreover, the IDC-PFC's capacity to exchange power in this study is 8 MW ($\overline{E}_C \times I_C$). Since both the IDC-PFC capacitor's DC voltage and its current are considered in the proposed droop gains, violating the IDC-PFC capacity limitation of exchange power is prevented.

In previous DC power flow studies with the presence of IDC-PFC [5,7,14,15,17], only the magnitude of the IDC-PFC capacitor's DC voltage ($\overline{E}_C$) was controlled by swinging the duty cycle (D) within a limited operational area. Moreover, the droop-control power-sharing strategies [9–13] have not considered the presence of any kind of IDC-PFC to study the benefits. However, in this paper, to avoid restrictions on the IDC-PFC's operation, adaptive droop is exerted as a new degree of freedom.

3. IDC-PFC operation analysis under duty cycle and variable droop

3.1. Three-terminal HVDC test Grid: A comparison study to [5]

The three-terminal HVDC test grid of CIGRE is studied in this section specifically to compare the results of the proposed droop strategy (as a new degree of freedom to contribute to the IDC-PFC's operation) to the results of [5] (which only had considered duty cycle for the IDC-PFC operation), see Fig. 4. The grid information is derived from [5]. The HVDC bus-*3* is a constant power bus (connected to an offshore wind farm) with a power of 800 MW, while the bus-*1* is a slack bus. The HVDC bus-*2* is connected to an onshore-side converter. The aims of this study are listed below:

- Firstly, since the IDC-PFC's master (t) and slave (u) HVDC cables are connected to the bus-*2* (which affects both cables' currents), the droop coefficient of the bus-*2* is considered to be variable (which was constant power bus in [5] with 400 MW power) to study the effect of variable droop on the behavior of the IDC-PFC. For this purpose, all the possible operation of the system is swept up for various feasible droop gains. Therefore, the main characteristics of the IDC-PFC are extracted with two degrees of freedom (duty cycle and droop gain).

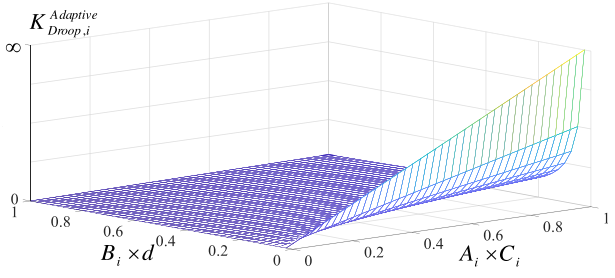

Fig. 3. 3D response of the proposed adaptive droop ($K^{Adaptive}_{Droop,i}$) concerning power/current and voltage deviation from nominal values.

- Secondly, the advantages of the proposed strategy are compared to the results of [5], and the broadened operational routes are analyzed. In other words, it is shown that the system can operate in an extensive route if the droop gain is chosen appropriately.
- Finally, a figure that segregates the widened operational area caused by IDC-PFC and the combination of IDC-PFC and variable droop is provided. This figure illustrates the widened operational area in detail.

3.2. DC power Flow of Three-Terminal test HVDC grid in the presence of IDC-PFC with variable droop

In this section, DC Power Flow (DC-PF) for the three-terminal HVDC test grid in the presence of variable droop gain is presented. Considering that the Bus-*1* is a slack-bus, the DC-PF can be stated as follows:

$$U_{DC,1} - U^{*}_{DC,1} = 0, \text{slack bus} \tag{15}$$

$$I_2 - \frac{P_2}{U_{DC,2}} = 0, I_3 - \frac{P^{*}_3}{U_{DC,3}} = 0 \tag{16}$$

$$I_1 - I_{12} - I_{13} = 0, I_2 + I_{12} + I_{23} = 0, I_3 + I_{13} - I_{23} = 0 \tag{17}$$

$$\frac{1}{R_{12}}(U_{DC,1} - (1-D)\overline{E}_C - U_{DC,2}) - I_{12} = 0 \tag{18}$$

$$\frac{1}{R_{13}}(U_{DC,1} - U_{DC,3}) - I_{13} = 0, \frac{1}{R_{23}}(U_{DC,3} - U_{DC,2} - D\overline{E}_C) - I_{23} = 0 \tag{19}$$

$$P_2 = -K_{Droop,2} \times (U_{DC,2} - U^{*}_{DC,2}) \tag{20}$$

$$P^{*}_3 = \frac{-U_{DC,2}U_{DC,3} - U_{DC,3}D\overline{E}_C + U^2_{DC,3}}{R_{23}} + \frac{-U_{DC,1}U_{DC,3} + U^2_{DC,3}}{R_{13}} \tag{21}$$

For the given DC-PF equations, the parameters $U^{*}_{DC,1}$,$U^{*}_{DC,2}$, P^{*}_3, R_{12}, R_{13}, and R_{23} are slack-bus reference DC voltage, the DC voltage reference value of adaptive-droop-controlled bus-*2*, constant power of bus-*3* (offshore wind farm), and resistances of *cable-1*, *cable-2*, and *cable-3*, respectively. Moreover, considering the active power balance of the IDC-PFC, the relation between duty cycle (D) and the droop of the bus-*2* ($K_{Droop,2}$) can be stated as follows:

$$P_2 = U_{DC,2}I_2 = -K_{Droop,2} \times (U_{DC,2} - U^{*}_{DC,2}), I_2 D - I_{12} = 0 \tag{22}$$

$$K_{Droop,2} = \frac{U_{DC,2}I_{12}}{D(U^{*}_{DC,2} - U_{DC,2})} \tag{23}$$

The presented DC-PF is solved by the Newton-Raphson method [14] in steady-state conditions.

3.3. 3D analysis of the IDC-PFC Characteristics: Duty cycle and droop gain are autonomous degrees of freedom

In this section, the contribution of variable droop as a new degree of freedom on the IDC-PFC's behavior is analyzed and the results are compared to those of the [5], see Fig. 5 and Fig. 6. The following 3D curves are the outputs of DC-PF studies sweeping all the possible duty cycle and droop gain of bus-*2* (in MATLAB 2023b: m.file coding).

By comparing the results of the IDC-PFC characteristics in Fig. 5 (with only duty cycle as a control variable) and Fig. 6 (with duty cycle and variable droop as control variables) in brief, the following advantages are achieved:

- Comparing Fig. 5 (a) and Fig. 6 (a), the DC voltage of bus-*2* is swingable within the range 203871 V $\leq U_{DC,2} \leq$ 205991 V(as the variable droop intervenes as an additional degree of freedom), while

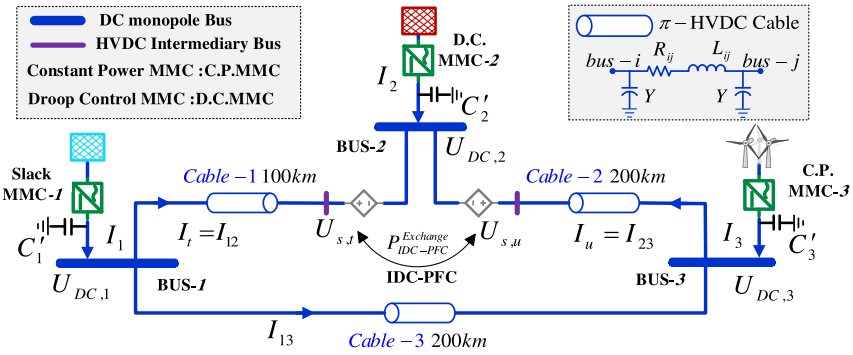

Fig. 4. Three-terminal test HVDC grid equipped with an IDC-PFC [5].

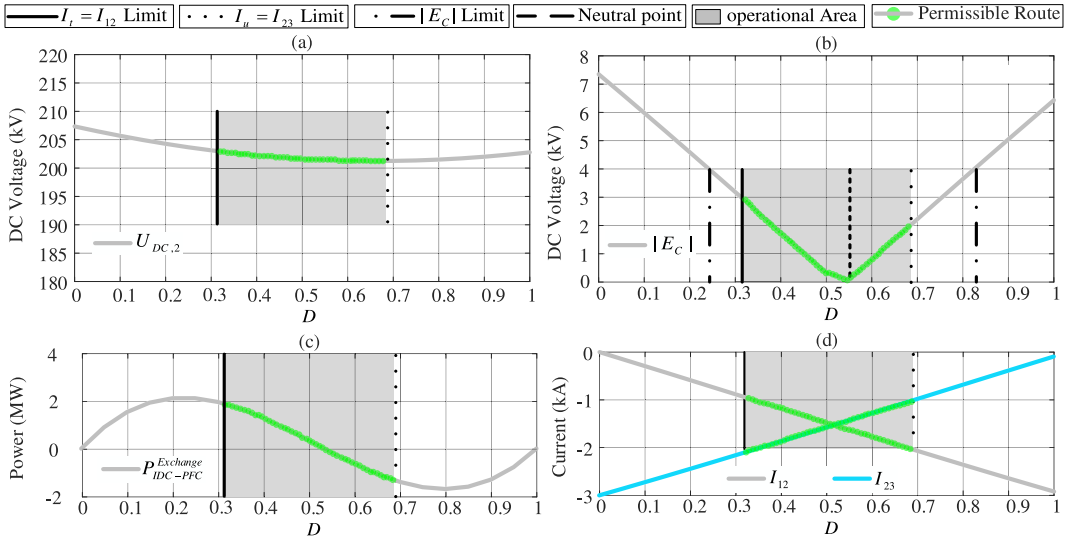

Fig. 5. IDC-PFC characteristics with duty cycle (one autonomous control variable) [5]: (a) DC voltage of bus-2, (b) IDC-PFC's capacitor's DC voltage, (c) Exchange power between master HVDC cable t and slave HVDC cable u, and (d) the currents of master and slave HVDC cables t and u.

it was 201854 V $\leq U_{DC,2} \leq$ 202674 V when only the duty cycle was in charge of the IDC-PFC operation.

- Comparing Fig. 5 (b) and Fig. 6 (b), the IDC-PFC's capacitor's DC voltage is fully swingable within its rated value (as the variable droop intervenes as an additional degree of freedom), while it was 0 V $\leq |\overline{E}_C| \leq$ 3155 V when only the duty cycle was in charge of the IDC-PFC operation.
- Comparing Fig. 5 (c) and Fig. 6 (c), the IDC-PFC's exchangeable power between HVDC cable *t* and HVDC cable *u* is swingable within the range -0.36699 MW $\leq P^{Exchange}_{IDC-PFC} \leq 6.45541$ MW (as the variable droop intervenes as an additional degree of freedom), while it was -1.23579 MW $\leq P^{Exchange}_{IDC-PFC} \leq 1.89367$ MW when only the duty cycle was in charge of the IDC-PFC operation. According to the result, the range of exchanged power has moved to the positive part, which means most power is transferred from the HVDC cable *u* to the HVDC cable *t*.
- Comparing Fig. 5 (d) and Fig. 6 (d), it is concluded that the swing-ability of the HVDC cable *t*'s DC current, has changed from $-2000 < I_t < -1000$ A (descending) to $-2000 < I_t < 2000$ A (as the variable droop intervenes as an additional degree of freedom). The swing-ability of the HVDC cable *u*'s DC current has shifted from $-2000 < I_u < -1000$ A (ascending) to $-254 \leq I_u \leq 574$ A (as the variable droop intervenes as an additional degree of freedom), respectively. Based on the results, the operation range for the HVDC cable *u* is slightly reduced with variable droop and duty cycle (828 A) which was (1000 A) with only duty cycle control. However, the HVDC cable *t* is operating at full capacity with the variable droop and duty cycle (4000 A) which was (1000 A) with only duty cycle control.
- More importantly, the duty cycle can be swung within 0.45268 $\leq D \leq$ 0.88248 (as the variable droop intervenes as an additional degree of freedom), while it was within 0.36854 $\leq D \leq$ 0.68871 where the only control variable was the duty cycle. Furthermore, the adaptive droop can be swung within 14.66527 $\leq K_{Droop,2} \leq$ 34.98027 considering system current and voltage limitations.

Finally, to obtain an overall outlook over the operational area of the three-terminal test HVDC grid, the following figure which segregates the widened operational areas thanks to the presence of IDC-PFC and both IDC-PFC with droop control strategy is illustrated, see Fig. 7. The grey squares are representative of the initial operational area where there is no installed IDC-PFC. Moreover, the white squares are the current limitations of the HVDC cables. Since the IDC-PFC redistributes extra currents of overloaded HVDC cables/lines to the neighborhood HVDC cables/lines, the white squares become operable. In the next, the blue squares are indicating the IDC-PFC capacitor's DC voltage limit ($\overline{E}_{C,n}$). Without an appropriate droop setting of the IDC-PFC's interconnected converters, the IDC-PFC capacitor's DC voltage might violate its limit. However, by assigning adaptive droop gains of the IDC-PFC's interconnected converters, the blue squares become operable. As it was shown in Fig. 6 (b) the IDC-PFC capacitor's DC voltage was completely operable thanks to the setting appropriate droop gain of the IDC-PFC's interconnected converters, the operational area of the system expanded

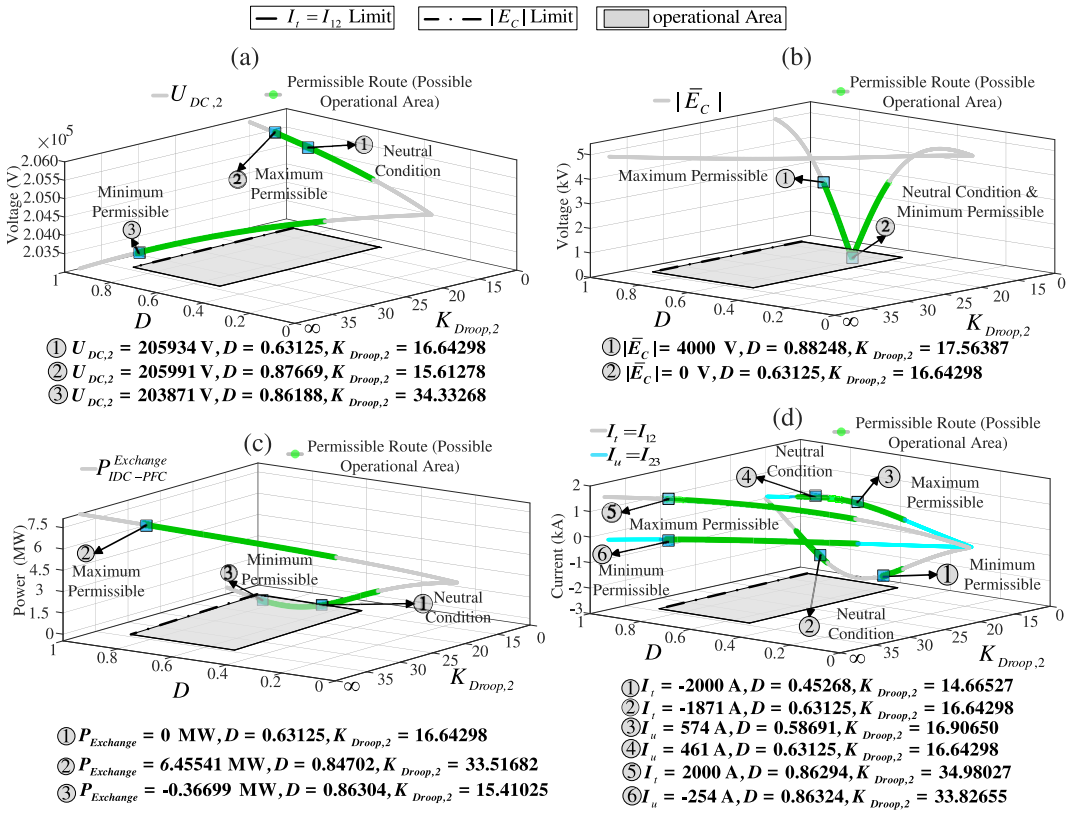

Fig. 6. IDC-PFC characteristics with variable droop and duty cycle (two autonomous control variables): (a) DC voltage of bus-*2*, (b) IDC-PFC's capacitor's DC voltage, (c) Exchange power between master HVDC cable *t* and slave HVDC cable *u*, and (d) the currents of master and slave HVDC cables *t* and *u*.

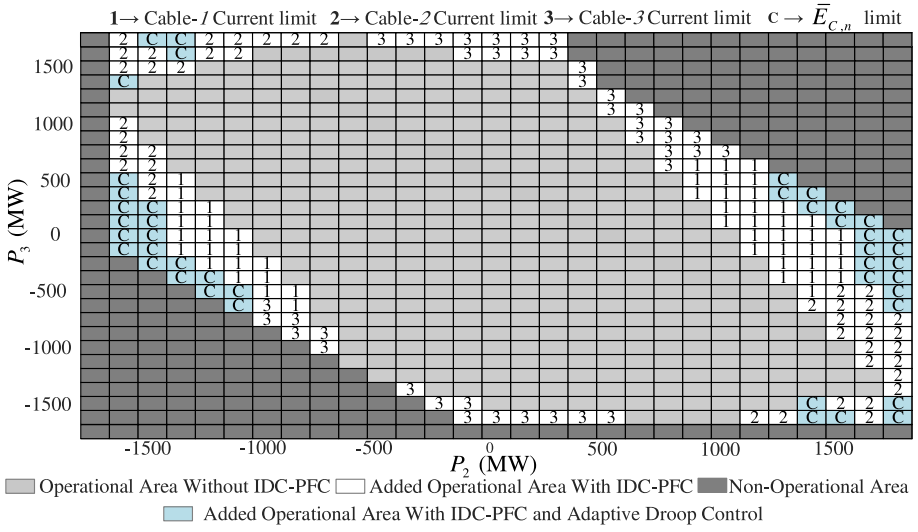

Fig. 7. Widened Operational area thanks to the combination of variable droop and duty cycle.

(the blue squares became operable), see Fig. 7. The darkest grey squares are non-operational areas where the power limitations of the converters will not allow further operation for the system.

4. State-Space HVDC system Modeling: Control structure & stability analysis

4.1. State-Space Modelling of Multi-Terminal HVDC grid with control structure

To assess the accuracy, efficiency, and role of the proposed strategy in escaping IDC-PFC's limitations, a control structure needs to be devised. For the dynamic simulations (in MATLAB-Simulink), the electromagnetic linearized transient model is implemented.

Taking the three-terminal HVDC grid as an example in Fig. 4, the state-space equations are as follows:

State-Space Equations:

To generate state-space equations, variables are considered to be operating at their assumed linearized points:

$$X \simeq X_0 + \frac{dX}{dt} \tag{24}$$

The parameters X, X_0, and dX/dt are variable, linearized point, and variation of the related variable, respectively. The HVDC transmission cables/lines are simulated in $\pi-$model, where R_{ij} and L_{ij} are the resistance and inductance of the cable/line, respectively. Nevertheless, the existence of the shunt resistors and capacitances (Y) does not contribute significantly to the results. Thus, they are eliminated from the space-state equations [16]. Finally, the linearized model of the presented space-state equations is depicted as (25).

$$\frac{dX}{dt} = AX + BU \tag{25}$$

The differential equations describing the modeled three-terminal test VSC-HVDC grid are illustrated as follows:

$$\frac{dU_{DC,1}}{dt} = \frac{1}{C_1'}\left(\frac{P_1}{U_{DC,10}} - \frac{U_{DC,1}P_{10}}{U_{DC,10}^2} - I_{12} - I_{13}\right) \approx 0, slack-bus \tag{26}$$

$$\frac{dU_{DC,2}}{dt} = \frac{1}{C_2'}\left(\frac{-K_{Droop,2}^{Adaptive}}{U_{DC,20}}U_{DC,2} + I_{12} + I_{23}\right) \tag{27}$$

$$\frac{dU_{DC,3}}{dt} = \frac{1}{C_3'}\left(\frac{P_3}{U_{DC,30}} - \frac{U_{DC,3}P_{30}}{U_{DC,30}^2} + I_{13} - I_{23}\right) \tag{28}$$

$$\frac{dI_{12}}{dt} = \frac{1}{L_{12}}(U_{DC,1} - U_{DC,2} - R_{12}I_{12} - (D_0 - 1)E_C - E_{C0}D) \tag{29}$$

$$\frac{dI_{13}}{dt} = \frac{1}{L_{13}}(U_{DC,1} - U_{DC,3} - R_{13}I_{13}) \tag{30}$$

$$\frac{dI_{23}}{dt} = \frac{1}{L_{23}}(U_{DC,2} - U_{DC,3} - R_{23}I_{23} - D_0E_C - E_{C0}D) \tag{31}$$

$$\frac{dE_C}{dt} = \frac{1}{C}((D_0 - 1)I_{12} + D_0I_{23} + (I_{120} + I_{230})D) \tag{32}$$

where A and B are state and input vector coefficients, respectively:

$$A = \begin{pmatrix} -\frac{P_{10}}{C_1'U_{DC,10}^2} & 0 & 0 & -\frac{1}{C_1'} & -\frac{1}{C_1'} & 0 & 0 \\ 0 & -\frac{K_{Droop,2}^{Adaptive}}{U_{DC,20}C_2'} & 0 & \frac{1}{C_2'} & 0 & \frac{1}{C_2'} & 0 \\ 0 & 0 & -\frac{P_{30}}{C_3'U_{DC,30}^2} & 0 & \frac{1}{C_3'} & -\frac{1}{C_3'} & 0 \\ \frac{1}{L_{12}} & -\frac{1}{L_{12}} & 0 & -\frac{R_{12}}{L_{12}} & 0 & 0 & \frac{1-D_0}{L_{12}} \\ \frac{1}{L_{13}} & 0 & -\frac{1}{L_{13}} & 0 & -\frac{R_{13}}{L_{13}} & 0 & 0 \\ 0 & \frac{1}{L_{23}} & -\frac{1}{L_{23}} & 0 & 0 & -\frac{R_{23}}{L_{23}} & -\frac{D_0}{L_{23}} \\ 0 & 0 & 0 & \frac{D_0-1}{C} & \frac{D_0}{C} & 0 & 0 \end{pmatrix} \tag{33}$$

$$B = \begin{pmatrix} \frac{1}{C_1'U_{DC,10}} & \frac{1}{U_{DC,20}C_2'} & 0 & 0 & 0 & 0 & 0 \\ 0 & 0 & 0 & -\frac{E_{C0}}{L_{12}} & 0 & -\frac{E_{C0}}{L_{23}} & \frac{I_{120}+I_{230}}{C} \end{pmatrix}^T \tag{34}$$

The parameter X is the state vector and the parameter $U(U = \{P_1, K_{Droop,2}^{Adaptive}, D\})$ is the input vector of the state-space equations. The parameters C_1', C_2', and C_3' are the converters' i, j, and k HVDC link capacitors, respectively. Moreover, the parameter C represents the IDC-PFCs capacitor. The parameter (P_1) decides how much power to be injected into the three-terminal HVDC grid. In addition, the duty cycle (D) and the adaptive droop gain of the bus-i ($K_{Droop,2}^{Adaptive}$) are the control variables.

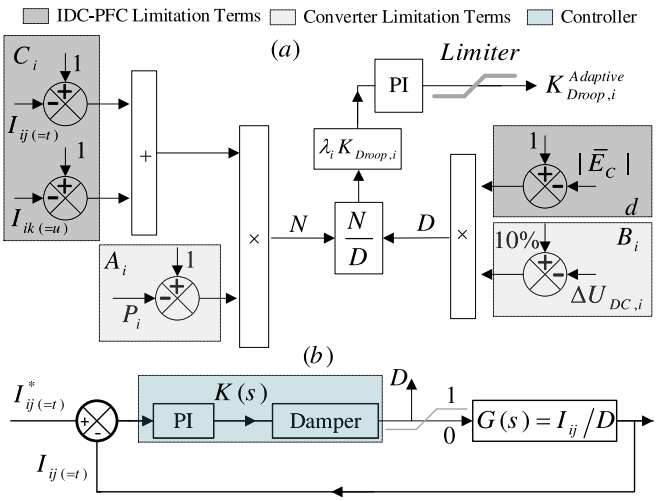

Fig. 8. Control Structure: (a) droop control structure for the bus-i and (b) master HVDC cable t current control structure.

For the bus-i, the control structure representing equation (12) is given, see Fig. 8 (a). In the proposed droop control, the terms A_i, B_i, C_i, and d represent the limits of the converter-i power, currents of master and slave HVDC cables where the IDC-PFC is installed, DC voltage deviation of the converter-i, and IDC-PFC capacitor's DC voltage, respectively. Fig. 8 (a) generates the equation (12) followed by a PI controller and a limiter. The droops for the bus-j and bus-k are set similarly following the equations (13) and (14), respectively. The PI controller is tuned/optimized by MATLAB 2023b PI-tuning toolbox. Also, the limiter considers the droop gain permissible operation route.

Based on the given state-space model, the transfer function that relates the duty cycle (D) to the master HVDC cable t current (I_{12}) is achieved ($G(s) = I_{12}/D$). Therefore, based on the transfer function $G(s)$, the following control structure for master HVDC cable t (I_{12}) current is shown in Fig. 8 (b). The following controller consists of four components including a PI controller (tuned by MATLAB Simulink Tuning Toolbox), a damper (for high-frequency oscillation damping), a limiter (maintains the duty cycle to operating within $0 \le D \le 1$) and finally, the transfer function extracted by state-space equations. The control system of Fig. 8 (b) sets the duty cycle to follow the given reference for the master HVDC cable t (I_{12}).

Moreover, to ensure the proposed adaptive droop control strategy works well, the measurement signals must be faster than the action of the control system to separate the dynamics of different control actions.

4.2. Stability analysis

In this section, the stability aspects of the proposed adaptive droop controller and master HVDC cable t current controller are analyzed for the three-terminal HVDC grid. To make sure the control structure with variable droop and duty cycle will operate smoothly, the closed-loop transfer function of the control structure is assessed.

$$\text{Closed - loop transfer function} = \frac{G(s)K(s)}{1 + G(s)K(s)} \tag{35}$$

In the following, the pole map of the closed-loop transfer function is illustrated, see Fig. 9. The pole map of the closed-loop transfer function depicts two sets of poles, one neutral and the other sensitive to the change of bus-2 droop gain. For the sensitive poles, it is seen that by swinging the droop value within the identified permissible operation

route ($14.66 < K_{Droop,2} < 34.98$), the poles move toward the stable part (more negative side), which shows that the proposed control structure is stable.

One important aspect of the proposed strategy is the interaction of the droop control dynamic with the duty cycle dynamic. According to the control structure in Fig. 8 and equation (35), there is only one transfer function that relates the master HVDC cable *t* current to the duty cycle. Therefore, the dynamics of the system are dictated by the existing transfer function. As the duty cycle imposes its dynamics on the output master HVDC cable *t* current, these dynamics directly show themselves in the adaptive droop control strategy. Therefore, since their dynamics are the same, there are no interactions between the duty cycle and adaptive droop control strategy.

5. Steady-State Analysis: Optimal-Adaptive −Droop-Controlled power Flow (OADC-PF)

5.1. Importance of applying OADC-PF in the presence of an IDC-PFC

The proposed adaptive droop control structure of Fig. 8 tries to adapt the droop value of the converters to avoid limitations of the IDC-PFC. However, this is not optimal. It is worthwhile knowing the optimal value of the converters' droops. In other words, the OADC-PF with the optimal results means that the converters' droops are set optimally, therefore, they contribute to the IDC-PFC limitation removal as much as possible.

For solving the optimization problem, Sequential Quadratic Programming (SQP) of MATLAB software is utilized. Moreover, Genetic Algorithm (GA) is also used to solve the optimization problem ensuring the results are global optimal points.

5.2. Power injection model of the IDC-PFC

It is a well-known method to generate the impact of the IDC-PFC in DC-PF formulations using power injection models (PIMs). The PIM formulations for the IDC-PFC are studied on the basis of the lumped-π model of the interconnected HVDC lines. The effect of IDC-PFC in the DC-PF formulations is achieved by comparing power equations in the presence and absence of IDC-PFC [17], as follows:

$$P(i) = -\left(\frac{(1-D)U_{DC,i}\overline{E}_C}{R_t} - \frac{DU_{DC,i}\overline{E}_C}{R_u}\right) \tag{36}$$

$$P(j) = \frac{(1-D)U_{DC,j}\overline{E}_C}{R_t} \tag{37}$$

$$P(k) = -\frac{DU_{DC,k}\overline{E}_C}{R_u} \tag{38}$$

In the equations (36)-(38), $P(i)$, $P(j)$, and $P(k)$ present the impacts of an IDC-PFC that are artificially injected into the buses i, j and k, respectively. These equations represent the effects of an IDC-PFC on DC power flow studies. For further information regarding the modeling process of an IDC-PFC, refer to [17].

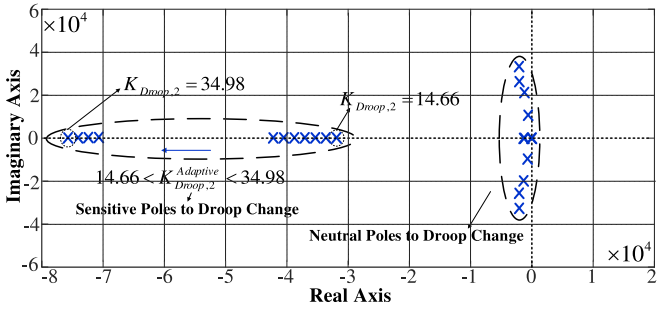

Fig. 9. Poles of closed-loop transfer function of the control structure.

5.3. Multi-Objective function & optimization problem

In this paper, two goals will be followed: (i) minimizing the DC voltage deviations of the HVDC grid's buses and (ii) minimizing the current index of all the HVDC cables and overhead lines. Thus, the DC voltage deviation term (F_V) and the current mitigation term (F_I) are described as below:

$$F_V = \sum_{i=1}^{N_{bus}} |(U_{DC,i} - 1)_i - 1|; i = 1, 2, 3, ..., N_{bus} \tag{39}$$

$$F_I = \sum_{t=1}^{N_{Line}} \frac{|I_{DC-t}|}{|I_{DC-t,\max}|}; t = 1, 2, 3, ..., N_{Line} \tag{40}$$

For the above equations, the parameters N_{bus} and N_{Line} indicate the number of HVDC buses and HVDC cable/overhead lines, respectively. The parameters I_{DC-t} and $I_{DC-t,\max}$ are the HVDC cable/ overhead line current and current limitation, respectively.

For more clarification, the term F_V demonstrates the HVDC buses' DC voltage deviation from their reference values (nominal values), while the term F_I is for avoiding bottleneck occurrence in HVDC cables/ overhead lines. The more deviation of the systems' voltages is from their nominal value, the more the system has a broad operational area. In other words, the system must have had a broader operational area to be able to deviate systems' DC voltages from their nominal values. Therefore, because the DC voltages of the buses are allowed to swing ($0.95 \le U_{DC,i} \le 1.05$), the DC voltage of each bus is subtracted to 1 and then the accumulated value is subtracted to 1 again, see equation (39). This will clarify whether the DC Power Flow (DC-PF) is able to find a proper solution in a broader operational area.

Moreover, the equation (40) illustrates the loading of the multi-terminal HVDC system. The less the term F_I is, the less the loading of the system is. In other terms, having a small F_I means the injected powers from the Offshore Wind Farm (OWF)s into the multi-terminal HVDC transmission system have been distributed in a reasonable manner. Thus, all the HVDC cables/lines contribute to carrying the produced bulk power to the onshore side rather than a small number of HVDC cables/lines carrying a great deal of power.

5.4. Equality and inequality constraints

The optimization problem is solved subject to several equality and inequality constraints. The inequality constraints include some operational terms including DC voltage ($U_{DC,i}$), currents (I_{DC-t}), onshore-side converter power (P_i), duty cycle (D), and IDC-PFC capacitor's DC voltage. On the other hand, equality constraints are the power balance of the HVDC grid and the IDC-PFC capacitor's DC voltage. The inequality and equality constraints are described as follows:

Inequality constraints:

$$U_{\min} < U_{DC,i} < U_{\max} \tag{41}$$

$$I_{DC-t} \le I_{DC-t,\max} \tag{42}$$

$$-P_{\max} \le P_i \le P_{\max} \tag{43}$$

$$0 \le D \le 1 \tag{44}$$

$$\overline{E}_{\min} \le \overline{E}_C \le \overline{E}_{\max} \tag{45}$$

The DC voltage boundaries are set to be within$U_{\min} = 0.95$ and$U_{\max} = 1.05$. In addition, the IDC-PFC capacitor's DC voltage is allowed to swing $0.05U_{DC,i}$($\overline{E}_{\min}$=-$0.05U_{DC,i}$ and$\overline{E}_{\max} = 0.05U_{DC,i}$). Further, the onshore-

side converters power can fluctuate between their rated values (per-units) ($P_{max} = -P_{min} = 1$).

Equality Constraints:

$$W_1 = \frac{Diag(U_{DC})U_{DC}}{R} - P = 0 \tag{46}$$

$$W_2 = T_i U_{DC,i} + T_j U_{DC,j} + T_k U_{DC,k} - \bar{E}_C = 0 \tag{47}$$

The parameter P presents the bus power vector of the whole HVDC grid and it consists of three terms: (i) power injected by OWFs, (ii) power injected/absorbed by onshore MMCs, and (iii) PIM of IDC-PFC's effect. The onshore MMCs power equation with the adaptive droop gain (12–14) is stated, as follows:

$$P = -\boldsymbol{K}_{\boldsymbol{Droop}}^{\boldsymbol{Adaptive}}(U_{DC} - U_{DC}^{*}) \tag{48}$$

As mentioned earlier, the droop gain ($\boldsymbol{K}_{\boldsymbol{Droop}}^{\boldsymbol{Adaptive}}$) of the onshore-side converters can vary optimally in accordance with the operating point of the grid.

6. Case study

In this section, different scenarios are defined to validate the effectiveness of the proposed methodology on the three-terminal HVDC grid and an eight-terminal HVDC grid derived from [18].

6.1. *Three-terminal HVDC grid of [5], see Fig. 4: Reference changing and power increment studies*

The first study, to challenge the ability of the IDC-PFC in current altering, it is aimed to empty/reverse the master HVDC cable-*1*'s current. According to Fig. 10 (a), the reference value of the HVDC cable-*1* (master HVDC cable) at (4 s) is changed from 0.39684 (p.u.) to −0.09 (p.u.) aiming to empty/reverse its current. However, the IDC-PFC

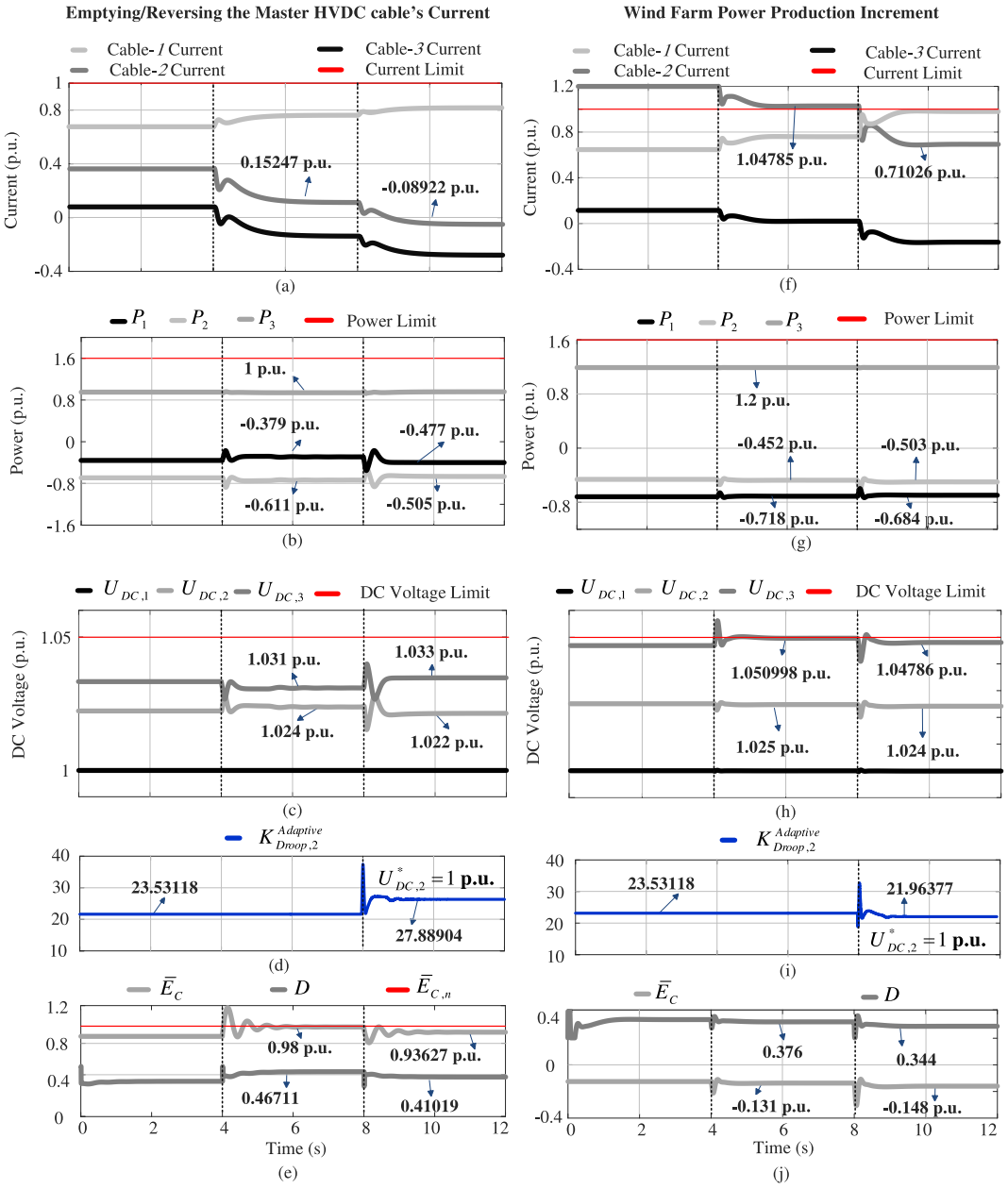

Fig. 10. Results of the proposed adaptive droop control strategy on the three-terminal HVDC grid: (a-e) results for current altering (emptying/reversing the master HVDC cable-*1*'s current), (f-j) results for power production increment of OWF connected to the bus-*3*.

capacitor's DC voltage ($\bar{E}_C$) gets closer to its limit and does not let the system follow the given reference (the current of the HVDC cable-*1* stops at 0.15247p.u.), see Fig. 10 (e). To escape this limitation, an appropriate droop gain is required to be set in a way to avoid IDC-PFC limitation. Therefore, the proposed adaptive droop control strategy is applied. According to Fig. 10 (d), at the time (8 s), the proposed strategy is applied, and the droop gain is changed from 23.53118 to 27.88904. Consequently, the IDC-PFC's capacitor's DC voltage is changed from almost 1p.u. to 0.93627p.u. which means the occurred limitation of the IDC-PFC is removed, see Fig. 10 (e). Also, the system can follow the given reference with the newly assigned droop gain, and the current of the master HVDC cable-*1* is changed to -0.08922p.u. (almost -0.09p.u.), see Fig. 10 (a).

In the second study, the power production of the OWF connected to the bus-*3* is increased by 20 %. According to Fig. 10 (f), the current of the master HVDC cable-*1* has increased to 1.210183p.u. which is overloaded by more than 20 % beyond its current limit. To avoid this, the reference value of the current of the master HVDC cable-*1* is set to be 0.7p.u. below its current limit. As is seen in Fig. 10 (f), the control system cannot follow the given reference because the DC voltage of the bus-*3* has been increased and hit its limit ($U_{DC,3}$ is 1.050998p.u.). To avoid this, the droop gain of the converter connected to the bus-*2* should be properly set. By applying the proposed strategy at the time (8 s), the droop gain of bus-*2* is changed from 23.53118 to 21.96377, see Fig. 10 (i). Following this change, the current master HVDC cable-*1* has been changed to the given desired reference (0.71026p.u.). More importantly, the DC voltage of bus-*3* which had caused the IDC-PFC to be limited to further operation, has changed from 1.050998p.u. to 1.04786p.u., which is below its limit.

An eight-terminal CIGRE HVDC test grid is studied in this section, see Fig. 11. In normal situations, offshore wind farms connected to the converters Cb-C2, Cb-C1, Cb-D1, and Cb-E1 produce constant powers of 1812 MW, 1000 MW, 1000 MW, and 1000 MW, respectively. Also, the fixed droop gains of the onshore-side converters Cb-A1, Cb-A2, Cb-B0, and Cb-B1 are $K_{Droop,1} = 57.58$, $K_{Droop,2} = 28.79$, $K_{Droop,4} = 57.58$, and $K_{Droop,7} = 28.79$, respectively. Moreover, the nominal values for per-unit calculations of power, DC voltage, and currents are 1812 MW, ±400 kV, and 2265 A, respectively. The parameters of the proposed HVDC test grid and the IDC-PFC are derived from [18].

To optimally place the IDC-PFC, the hybrid method of [19,20], known as max flow- min cut theory and sensitivity analysis are utilized.

6.2. Eight-terminal HVDC grid under HVDC Cable-5 Fault/Outage

OWF 5 (B0-C1) and OWF 3 (B0-C2) which are connected by HVDC cable-*5* are away from onshore MMCs. Regarding this, tripping HVDC cable-*5* might cause strict overloading in other HVDC cables or overhead lines. Based on Fig. 12, the HVDC cable-*5* outage causes HVDC cable-*7* to be operating at -1.24p.u., which is beyond its limit. According to Fig. 13, the IDC-PFC capacitor's DC voltage does not let the IDC-PFC inject voltage to the HVDC cable-*8* further to absorb the extra current of HVDC cable-*7* (the IDC-PFC's capacitor has been saturated). Moreover, the DC voltage of bus-*6* (Bb-6) is close to its limit, see Fig. 14 (b). This means that the IDC-PFC is trapped within the limitations of the system. At this point, the proposed adaptive droop setting is required. Based on Fig. 14 (c), at the time (6 s), the droop values of the MMC-*1* (Cb-A1), MMC-*2* (Cb-A2), MMC-*4* (Cb-B1), and MMC-*7* (Cb-B0) are reset by the proposed adaptive droop control strategy. From Fig. 14 (c), the droop values of MMC-*1* (Cb-A1) and MMC-*4* (Cb-B1) have changed from 57.5 to 63.14 and 44.3, respectively, while those of MMC-*2* (Cb-A2) and MMC-*7* (Cb-B0) have changed from 28.7 to 25.8 and 42.6, respectively. To avoid the IDC-PFC's capacitor DC voltage limitation, the droop of MMC-*7* (Cb-B4) has increased to operate toward a constant voltage bus. More importantly, the increased droop of MMC-*7* (Cb-B4), will pave the way for reasonable power sharing between the converter and the HVDC cables 7, 8, and 9. On the other hand, other MMCs have changed their droops to

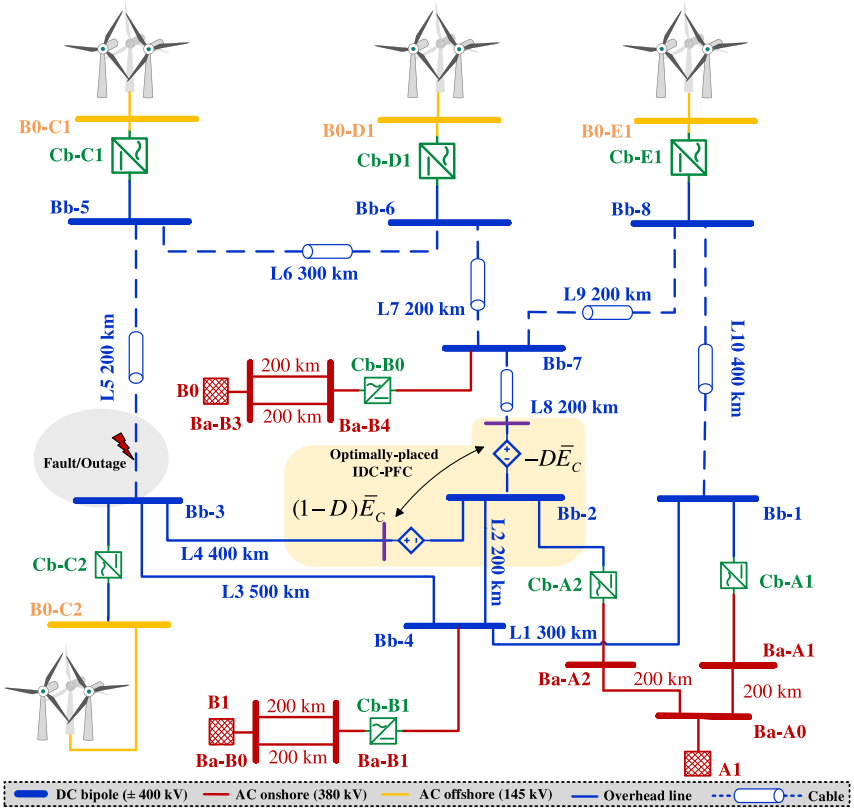

Fig. 11. Eight-terminal HVDC grids with IDC-PFC mounted on HVDC cable-*8* and HVDC overhead line-*4*. Studies are conducted for HVDC cable-5 fault/outage.

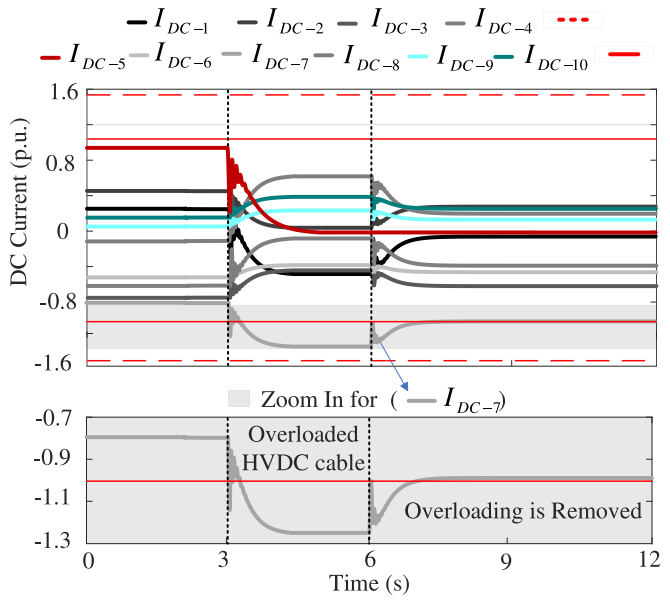

Fig. 12. HVDC cable-*5* fault-outage in the eight-terminal HVDC grid: Currents of HVDC cables and overhead lines (Dashed and solid red lines are over-headlines' and cables' currents' limits, respectively). (For interpretation of the references to colour in this figure legend, the reader is referred to the web version of this article.)

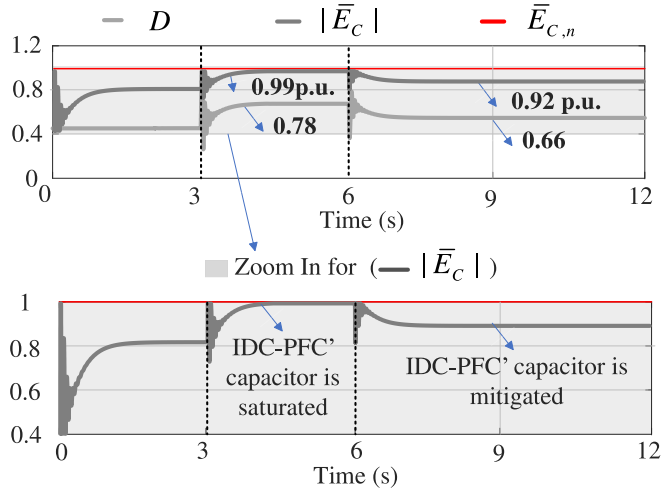

Fig. 13. Duty cycle and IDC-PFC capacitor's DC voltage (red line is IDC-PFC capacitor's DC voltage limit). (For interpretation of the references to colour in this figure legend, the reader is referred to the web version of this article.)

compensate for power mismatch in the system. Now, the HVDC cable-*7* is operating at -0.99p.u. which is almost its limit, and it is not overloaded anymore.

6.3. Steady-State Analysis: OADC-PF for eight-terminal HVDC grid under HVDC Cable-5 Fault/Outage

This section compares the dynamic results of the proposed adaptive droop-control strategy to the results of the OADC-PF with consideration of the HVDC cable-*5* outage. In this section, the difference between optimal and non-optimal DC power flow are discussed. Optimally set adaptive droop values of converters with the proposed strategy will maximize IDC-PFC operability. The results for OADC-PF are collected in Table 1.

According to Table 1, the results are very similar to those of the

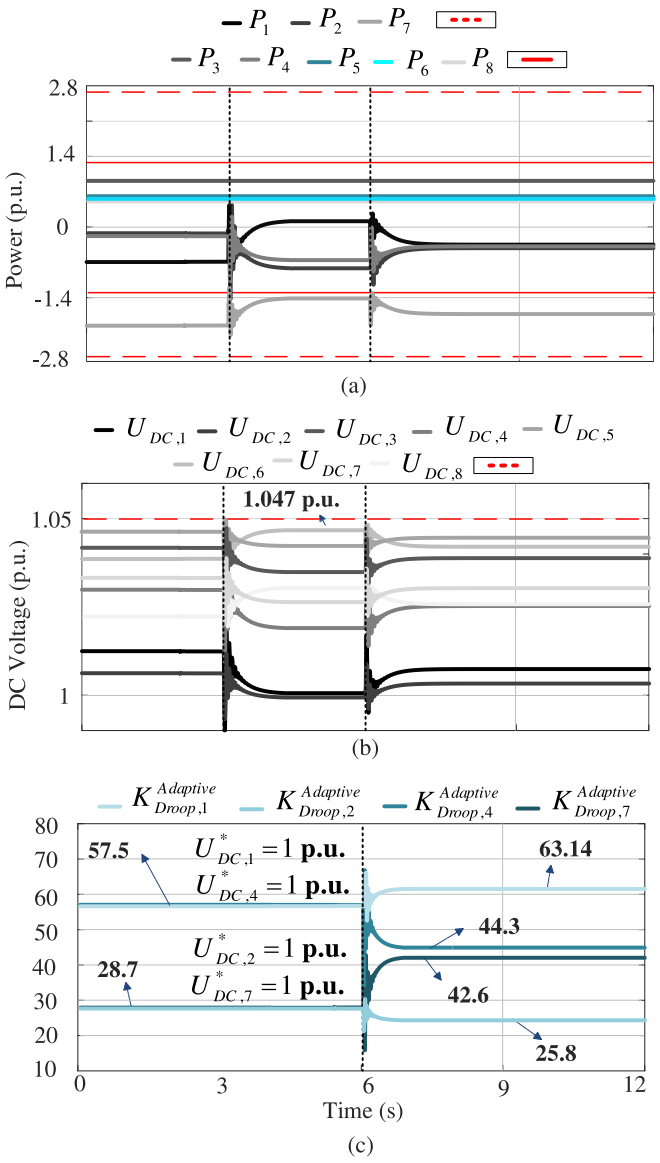

Fig. 14. (a) Converters' powers of MMCs (Dashed and solid red lines are converters' power limit), (b) DC voltages (dashed red line is DC voltage limit), and (c) Adaptive droop values. (For interpretation of the references to colour in this figure legend, the reader is referred to the web version of this article.)

dynamic results in section VI. C. For example, the tripping of HVDC cable-*5* has caused the HVDC cable-*7* to be overloaded in both dynamic and steady-state studies. Based on Fig. 12 and Table 1, after applying the proposed droop control strategy, the current of HVDC cable-*7* has changed from -1.24p.u. to -0.99p.u. in the proposed dynamic control, while it has changed from -1.13442p.u. to -0.92036p.u. with the proposed OADC-PF. This shows that the OADC-PF has found much more reasonable results as the HVDC cable-*7*'s current reduced more than dynamic results. Moreover, based on Fig. 14 (c) and Table 1, after applying the proposed droop control strategy, the droop values of MMC-*2* (Cb-A2) and MMC-*4* (Cb-B1) have decreased, while for the MMC-*1* (Cb-A1) and MMC-*7* (Cb-B0) have increased in the proposed dynamic control and the OADC-PF with a similar pattern to avoid IDC-PFC capacitor's restriction.

Moreover, from Table 1, the DC voltage deviation term (F_V) and the current mitigation term (F_I) have been decreased significantly with the proposed adaptive droop control strategy compared to fixed droop operation. For instance, the DC voltage deviation term (F_V) was 0.99999 for fixed droop operation, while it has decreased to 0.72946 with the

Table 1
Eight-terminal CIGRE Test Grid's OADC-PF Results.

m.file Result	**Scenario 1: Uncompensated & compensated HVDC Cable 5 outage**			
Bus	**Uncom**[a]	**Uncom**[a]	**Com**[b]	**Com**[b]
	DC Voltage	**Bus Power**	**DC Voltage**	**Bus Power**
1	0.99432	0.07960	1.02499	−0.33833
2	0.98370	−0.59685	1.02019	−0.24915
3	0.99998	1	1.04682	1
4	0.98587	−0.68860	1.02499	−0.30900
5	1.02183	0.55187	1.05000	0.55187
6	1.01228	0.55187	1.04123	0.55187
7	1.00007	−1.44165	1.03007	−1.68061
8	1.00208	0.55187	1.03219	0.55187
Line-*t*:	**Current**	**C.L**[d]	**Current**	**C.L**[d]
1	−0.43648	±1.54525	−0.00273	±1.54525
2	0.16758	±1.54525	0.37205	±1.54525
3	−0.43219	±1.54525	−0.67624	±1.54525
4	0.56666	±1.54525	0.27764	±1.54525
5	0	±1	0	±1
6	−0.59233	±1	−0.54323	±1
7	**−1.1344(√)**[c]	±1	−0.92036	±1
8	−0.12537	±1	−0.40325	±1
9	0.18688	±1	0.19693	±1
10	0.36074	±1	0.33453	±1
IDC-PFC	$D = 0.81883\overline{E}_C = 0.99264$ (√)[f]		$D = 0.40775\overline{E}_C = 0.69748$	
$K_{Droop,1}$	Fixed = 57.5		**Adaptive-Optimal = 63.8**	
	$U^*_{DC,1} = 0.99293$		$U^*_{DC,1} = 1.01968$	
$K_{Droop,2}$	Fixed = 28.7		**Adaptive-Optimal = 26.6**	
	$U^*_{DC,2} = 0.96290$		$U^*_{DC,2} = 1.01079$	
$K_{Droop,4}$	Fixed = 57.5		**Adaptive-Optimal = 49.5**	
	$U^*_{DC,4} = 0.97404$		$U^*_{DC,4} = 1.01873$	
$K_{Droop,7}$	Fixed = 28.7		**Adaptive-Optimal = 39.4**	
	$U^*_{DC,7} = 0.98285$		$U^*_{DC,7} = 0.98734$	
F_I	3.43714[i]	3.44654[h]	3.37272[i]	3.39011[h]
F_V	0.99999[i]	1[h]	0.72946[i]	0.72864[h]

[a] Uncompensated,
[b] Compensated,
[c] Over Current (√),
[d] Current Limit, [e]Over Power Converter (√), [f] limit (√), [g]DC Voltage limit,
[h] GA,
[i] SQP.

proposed adaptive droop strategy. Additionally, the current mitigation term (F_I) was 3.43714 for fixed droop operation, while it has become 3.37272 with the proposed adaptive droop strategy. This shows that the voltage of the buses and the currents of the cables/lines can change more without violating the IDC-PFC and system's restrictions.

Future Work:

The proposed strategy can also be further manipulated for other purposes. Some of the potential uses can be classified as follows:

- **Applicable for different types of DC Power Flow Controllers:**

The proposed method for widening the operational area of an IDC-PFC in this paper was applied to a dual-port Interline DC Power Flow Controller (IDC-PFC) with 6 switches and a capacitor. However, complex topologies of DC Power Flow Controllers (DC-PFC)s emerged in recent studies with multi-port branch connections. The proposed method can also be extended for the flexible operation of multi-port DC-PFCs.

Moreover, this paper's proposed method applies to different types of DC-PFCs including series and cascaded DC-PFCs to expand the flexibility of their control variables.

- **Integrating the proposed method into the operation of HVDC circuit breakers**

This idea can be combined with the performance of an HVDC circuit breaker to enhance its capability to DC Power Flow (DC-PF) and transient current/power of the HVDC cables/lines. In other words, the operation of an HVDC circuit breaker can be integrated into the converters' droop gains to achieve a safe and reliable performance.

- **Battery Energy Storage Systems (BESS)s**

The proposed method can also be applied to BESS for power flow control, reactive power provision, frequency regulation, etc.

7. Conclusion

In this paper, a droop-controlled strategy is proposed to widen the IDC-PFC's operational area in MMC/VSC-based HVDC systems. It was analyzed that the IDC-PFC's operation is strongly restricted by several HVDC cables/lines' currents or bus/IDC-PFC capacitor's DC voltage. These restrictions prevent the IDC-PFC's effective potential in current/power control. To avoid this problem, one effective way is to carry out adaptive droop control, which considers IDC-PFC's limitations. Thus, the impact of a variable droop control of converters on the behavior of the IDC-PFCs in the three-terminal CIGRE test HVDC test grid was assessed and compared to the results of [5] where only the duty cycle was in charge of IDC-PFC control. It was shown that by intervening the variable droop in power flow equations in the presence of the IDC-PFC, a much wider operational area is conceivable for the IDC-PFC. Afterward, an adaptive droop control structure is proposed to embrace the limitations of the IDC-PFC which relates the operation of the IDC-PFC to the operation of the MMC/VSC converters. The proposed adaptive droop strategy will avoid those limitations in accordance with the system's operating point. Finally, the validity of the proposed method was evaluated through the three and eight-terminal CIGRE HVDC test grid.

CRediT authorship contribution statement

Mirhamed Pourmirasghariyan: Writing – review & editing, Writing – original draft, Visualization, Validation, Software, Resources, Methodology, Investigation, Formal analysis, Data curation, Conceptualization. **G.B Gharehpetian:** Writing – review & editing, Writing – original draft, Visualization, Validation, Supervision, Conceptualization. **Oriol Gomis-Bellmunt:** Writing – review & editing, Writing – original draft, Visualization, Validation, Methodology, Investigation, Conceptualization. **David Campos-Gaona:** Writing – review & editing, Writing – original draft, Visualization, Validation, Supervision, Data curation. **Panagiotis N. Papadopoulos:** Writing – review & editing, Writing – original draft, Visualization, Validation, Supervision, Methodology.

Declaration of competing interest

The authors declare that they have no known competing financial interests or personal relationships that could have appeared to influence the work reported in this paper.

Data availability

No data was used for the research described in the article.

References

[1] Hassan SJU, Mehdi A, Haider Z, Song JS, Abraham AD, Shin G, et al. Towards medium voltage hybrid AC/DC distribution systems: architectural topologies, planning, and operation. Int J Electr Power Energy Syst 2024;159.
[2] Xu B, Gao H, Peng F. Adaptive current injecting strategy for VSC-HVDC connected offshore wind farms during symmetrical faults. Int J Electr Power Energy Syst 2024;157.

[3] Huang H, Zhou M, Zhang S, Zhang L, Li G, Sun Y. Exploiting the operational flexibility of wind integrated hybrid AC/DC power systems. IEEE Trans Power Syst 2021;36(1):818–26.
[4] Zhang S, et al. A hybrid modular interline current flow controller for meshed HVDC grids. IEEE Trans Ind Electron 2022;69(10):10055–65.
[5] Sau-Bassols J, Prieto-Araujo E, Gomis-Bellmunt O. Modelling and control of an interline current flow controller for meshed HVDC grids. IEEE Trans Power Delivery 2017;32:11–22.
[6] Zhang F, Bieber L, Zhang Y, Li W, Wang L. A multi-port DC power flow controller integrated with MMC stations for offshore meshed multi-terminal HVDC grids. IEEE Trans Sustainable Energy 2023;14(3):1676–91.
[7] Heidary Yazdi SS, Milimonfared J, Fathi SH, Rouzbehi K. Optimal placement and control variable setting of power flow controllers in multi-terminal HVDC grids for enhancing static security. Int J Electr Power Energy Syst 2018;102:272–86.
[8] Gomis-Bellmunt O, Sau-Bassols J, Prieto-Araujo E, Cheah-Mane M. Flexible converters for meshed HVDC grids: from flexible AC transmission systems (FACTS) to flexible DC grids. IEEE Trans Power Delivery 2020;35(1):2–15.
[9] Rouzbehi K, Miranian A, Candela JI, Luna A, Rodriguez P. A generalized voltage droop strategy for control of multiterminal DC grids. IEEE Trans Ind Appl 2015;51(1):607–18.
[10] Wang Y, Wen W, Wang C, Liu H, Zhan X, Xiao X. Adaptive voltage droop method of multiterminal VSC-HVDC systems for DC voltage deviation and power sharing. IEEE Trans Power Delivery 2019;34(1):169–76.
[11] Wang W, Li Y, Cao Y, Häger U, Rehtanz C. Adaptive droop control of VSC-MTDC system for frequency support and power sharing. IEEE Trans Power Syst 2018;33(2):1264–74.
[12] Wei J, et al. Coordinated droop control and adaptive model predictive control for enhancing HVRT and post-event recovery of large-scale wind farm. IEEE Trans Sustainable Energy 2021;12(3):1549–60.
[13] Vijay AS, Doolla S. Performance of droop control techniques under nonlinear loading conditions: uniform and nonuniform configurations. IEEE Syst J 2021;15(2):2245–56.
[14] Abbasipour M, Milimonfared J, Yazdi SSH, Rouzbehi K. Power injection model of IDC-PFC for NR-based and technical constrained MT-HVDC grids power flow studies. Electr Pow Syst Res 2020;182.
[15] Sau-Bassols J, Zhao Q, García-González J, Prieto- Araujo E, Gomis-Bellmunt O. Optimal power flow operation of an interline current flow controller in an hybrid AC/DC meshed grid. Electr Pow Syst Res 2019;177.
[16] Pérez-Rúa J-A, Stolpe M, Cutululis NA. Integrated global optimization model for electrical cables in offshore wind farms. IEEE Trans Sustainable Energy 2020;11(3):1965–74.
[17] Abbasipour M, Liang X. Power flow study of MT-HVDC grid compensated by multiport interline DC power flow controller. IEEE Trans Ind Appl 2023;59(4):4786–96.
[18] Vrana TK, Yang Y, Jovcic D, Dennetière S, Jardini J, Saad H. The CIGRE B4 DC grid test system. Electra 2013;270(9):10–9.
[19] Pourmirasghariyan M, Milimonfared J, Yazdi SSH, Rouzbehi K. Hybrid method for optimal placement of DC-PFCs to enhance static security of VSC-HVdc grids. IEEE Syst J 2022;16(3):4839–48.
[20] Pourmirasghariyan M, Milimonfared J, Yazdi SSH, Biglo AHA, Rouzbehi K. Application of max flow-min cut theory to find the best placement of electronic-based DC-PFCs for enhancing static security in MT-HVDC meshed grids. In: 2022 30th International Conference on Electrical Engineering (ICEE). IEEE; 2022. p. 23–8.